Research Article Vol. 10, No. 6 / 1 June 2020 / Optical Materials Express 1405
Optical Materials EXPRESS

Electro-optic liquid crystal device employing two-dimensional WSe_2 as the planar-alignment layers

RAJRATAN BASU* AND LUKAS J. ATWOOD

Department of Physics, Soft Matter and Nanomaterials Laboratory, The United States Naval Academy, Annapolis, MD 21402, USA
*basu@usna.edu

Abstract: Two-dimensional (2D) tungsten diselenide (WSe_2) nanosheets were transferred onto indium tin oxide (ITO) coated glass slides. Two such 2D WSe_2-covered ITO glass slides were placed together to fabricate an electro-optic liquid crystal (LC) cell. A nematic LC inside this WSe_2-based device obtains uniform planar-alignment. The coherent overlay of the LC molecules along the armchair direction on the WSe_2 lattice leads to this planar-alignment at the molecular scale. This WSe_2-based LC device exhibits the typical electro-optical effect on the application of an electric field. A sharp Fréedericksz transition of the nematic director from this electro-optical effect confirms that the 2D WSe_2 provides sufficient planar anchoring energy in the device. Finally, the WSe_2/ITO slide exhibits more optical transparency than a standard polyimide alignment layer/ITO slide.

1. Introduction

Monolayer tungsten diselenide (WSe_2) is a highly stable two-dimensional (2D) semiconductor [1,2,3,4] whose crystal structure is shown in Fig. 1(a). Here we experimentally demonstrate that 2D WSe_2 can impose planar-alignment to a nematic liquid crystal (LC) in an electro-optic device. Optically anisotropic LC materials are vastly employed in modern electro-optical display technology. Conventionally, unidirectionally rubbed polyimide (PI) layers are used as the planar-alignment agent in standard optically transmissive liquid crystal displays (LCDs) [5], where the LC molecules align with the alkyl side chains along the rubbing direction on the PI layers, achieving a homogeneous (*i.e.*, uniform planar) director ($\hat{n}$) profile inside the device [6]. However, this LC alignment process using the rubbed PI layers triggers some disadvantages. For example, a large distribution of pre-tilt angles of the LC developed due to the uneven mechanical rubbing process on the PI layers generates non-uniform brightness in the LCD panel [5]; free ion impurities stemming from the PI alignment layers can contaminate the LC [7]; and the residual fiber dust from the rubbing process of the PI layers increases the contaminants in the LC [5]. Moreover, the organic PI layers are responsive to UV light and high temperature, and therefore, the alignment characteristics are affected when the PI-based LC devices are exposed to UV light and high temperature [8,9]. Thus, there exists an important research direction to explore various LC-substrate anchoring phenomena to develop alternate LC alignment methods, such as photoalignment method [10], epitaxial alignment technique using inorganic alignment agents, e.g., graphene [11,12,13,14] and hexagonal boron nitride [15,16,17,18], oblique SiO evaporation technique [5], and microgroove grating surface fabrication method [5] to name a few.

Recent studies show that the crystallographic orientation of 2D hexagonal transition metal dichalcogenides (TMDs), such as $MoSe_2$ and WSe_2, can be characterized by the alignment process of an LC on their surfaces [19,20]. The LC aligns on the 2D hexagonal nanostructures, including WSe_2, due to the epitaxial interaction between the LC's benzene rings and the honeycomb crystal structure of the 2D hexagonal nanostructures [19,20]. It has been found using the density functional calculations that the alignment of the LC molecules has a distinct preferential direction along the armchair direction on the WSe_2 lattice with an adsorption energy ~ 1.708 eV/molecule

#393296 https://doi.org/10.1364/OME.393296

Received 20 Mar 2020; revised 20 Apr 2020; accepted 11 May 2020; published 18 May 2020

Optical Materials EXPRESS

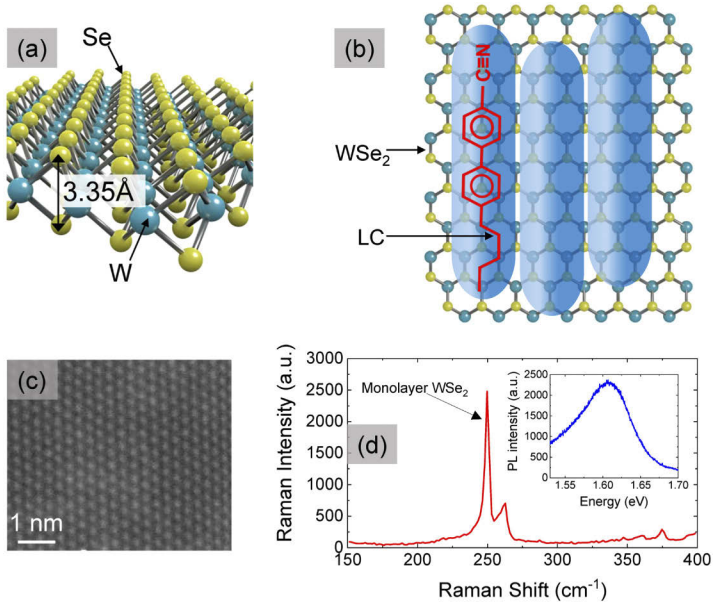

Fig. 1. (a) Schematic representation of the monolayer WSe_2 crystal structure. (b) Schematic representation of the planar alignment of the LC along the armchair direction the monolayer WSe_2 nanostructure. (c) The transmission electron microscopy (TEM) of WSe_2 on a TEM grid. (d) Raman spectroscopy of monolayer WSe_2 on ITO; inset: photoluminescence (PL) emission of monolayer WSe_2 on ITO.

[19]. Here we report that the 2D WSe_2 can function as the planar-alignment agent, without any additional PI layers, in an LC device that exhibits the required electro-optical effect on the application of a voltage.

2. Experiments, results, and discussion

In this section, we present (a) the fabrication of the WSe_2-based planar LC cell, (b) the electro-optical effect of the LC in the cell, and finally, (c) the optical transmission spectroscopy of WSe_2/ITO slide.

2.1. Fabrication of the electro-optic LC cell employing 2D WSe_2 as the planar-alignment agent

In a WSe_2 lattice, each selenium (Se) atom is bonded to three tungsten (W) atoms in a pyramidal geometry, as shown in Fig. 1(a). The top-view hexagonal lattice structure of WSe_2 is shown in Fig. 1(b). According to Ref. [19], the LC molecules align better along the armchair direction due to the epitaxial interaction—which is illustrated in Fig. 1(b). This spontaneous planar-alignment mechanism of the LC molecules along the armchair direction on this 2D WSe_2 lattice is the fundamental principle in our experiment for employing the monolayer WSe_2 as the planar-alignment agent in this electro-optic LC device. In [19], the WSe_2 was deposited on a silicon substrate, and no electro-optic LC device was designed to see any electric field-induced switching effect. In our experiment, we have transferred the monolayer WSe_2 on ITO substrates, and two such WSe_2/ITO slides were utilized to design an electro-optic LC cell where an electric field was applied.

We have first conducted the following experiments to investigate the 2D WSe_2 lattice-induced planar-alignment of the LC. High-quality chemical vapor deposition (CVD) grown monolayer

Optical Materials EXPRESS

WSe_2 film covered across c-cut sapphire was obtained from *2Dsemiconductors Inc*. The transmission electron microscopy (TEM) image of 2D WSe_2 on a TEM grid in Fig. 1(c) confirms the highly crystalline nature of the monolayer WSe_2 samples. The monolayer WSe_2 films from the sapphire substrates were then transferred onto several indium tin oxide (ITO) coated glass substrate employing the standard polymethyl-methacrylate (PMMA) aided wet transfer method [21,22]. Only 1×1 cm^2 area was covered with the transferred monolayer WSe_2 on the 2.5×2.5 cm^2 ITO coated glass substrates. We reached this size limit because only 1×1 cm^2 monolayer WSe_2 could be produced by *2Dsemiconductors Inc*. After the transfer process, the Raman spectroscopy in Fig. 1(d) and the photoluminescence (PL) emission in the inset in Fig. 1(d) confirm the presence of monolayer WSe_2 on the ITO slide [23,24]. A Raman microscope (IDRaman micro, *Ocean Optics, Inc.*) with a 532 nm excitation laser was used to study the Raman spectroscopy. The PL emission was studied using a QEPRO-FL spectrometer (*Ocean Optics, Inc.*) with a 2.5 mW and 532 nm excitation laser.

Figure 2(a) shows the picture of an ITO glass substrate with monolayer WSe_2 on it. A thin layer of LC was produced by putting down a small droplet of LC E7 ($T_{NI} = 60.5°C$, *EMD Millipore Corporation*) on the WSe_2/ITO slide, which was pre-heated at 70°C to bring the LC droplet in the isotropic phase. The LC droplet was then gently blowing away by a dust blower and slowly cooled down in the nematic phase. The thin LC layer was present on the monolayer WSe_2 as well as on the bare ITO area.

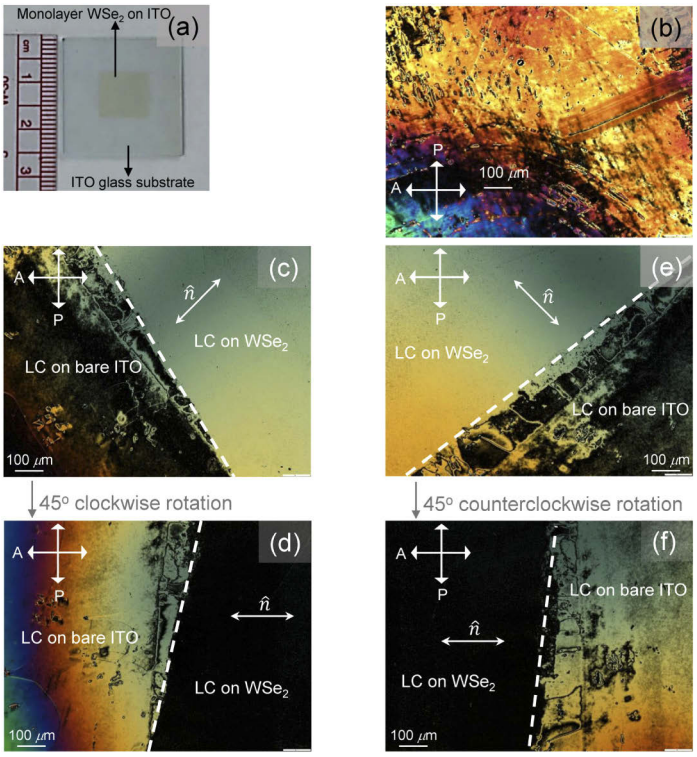

Fig. 2. (a) Picture of the monolayer WSe_2 on an ITO substrate. (b) Crossed-polarized micrograph of unaligned LC on the bare ITO substrate. (c), (d) Crossed-polarized micrograph and its 45° rotated state, respectively, of the LC on the WSe_2/ITO substrate revealing uniform planar-alignment of the LC on the monolayer WSe_2 film and unaligned LC on the bare ITO region. (e), (f) Crossed-polarized micrograph and its 45° rotated state, respectively, of the same LC sample at a different edge of the monolayer WSe_2 film on the ITO substrate.

Optical Materials EXPRESS

A crossed-polarized optical microscope (Olympus BX61) was used to study the alignment of the LC on the monolayer WSe_2 film. Figure 2(b) shows the LC texture on the bare ITO substrate. The presence of multiple colors in this micrograph reveals that the LC does not achieve a uniform planar-aligned state on the bare ITO substrate. The micrograph in Fig. 2(c) exhibits the LC texture both on the monolayer WSe_2 film and on the bare ITO substrate. The white dashed line presents the edge of the monolayer WSe_2 film on the ITO substrate. The right side of the white dashed line shows that the LC achieves a uniform planar-aligned state on the WSe_2 film—where $\hat{n}$ is oriented at 45° with the crossed polarizers, producing a bright uniform texture with a maximum transmitted intensity. The small dark spots on the aligned LC texture are PMMA residues from the WSe_2 transfer process. These tiny PMMA-induced defects do not affect the overall LC alignment on the WSe_2 film. The left side of the white dashed line shows the randomly oriented LC domains on the bare ITO substrate. After the slide is rotated clockwise through 45° under the crossed-polarized microscope, the uniform planar-aligned LC on the WSe_2 film exhibits a dark uniform texture since $\hat{n}$ is now oriented parallel to the analyzer, as shown in the micrograph in Fig. 2(d). Figure 2(e) shows the LC texture at a different edge of the monolayer WSe_2 film on the ITO substrate. Similar to the previous one, a 45° rotated state is shown in the micrograph in Fig. 2(f). This experiment establishes that the monolayer WSe_2 film imposes uniaxial planar-alignment (*i.e.*, homogeneous alignment) on the LC due to the epitaxial interaction. It is important to note here that on a single WSe_2 2D crystal, the LC molecules can assume three different orientations separated by 60 degrees due to the hexagonal symmetry. However, the micrographs shown in Figs. 2(c), 2(d), 2(e), and 2(f) clearly demonstrate that it is possible to get a reasonably large uniform LC domain with unidirectional planar-alignment (without any three-fold alignment degeneracy) on the WSe_2 film. We have not seen any misalignment. We believe this was achieved because of our LC coating technique—where a dust blower was used to gently blow the LC droplet in one direction from one side to the other on the t WSe_2/ITO slide.

A WSe_2-based cell (with a cell-gap $d = 16.8$ μm) was prepared by placing together two WSe_2/ITO glass substrates with the WSe_2 sides facing each other. The cell was filled with LC E7 in the isotropic phase by capillary injection from one opening and gentle vacuum suction from the other opening to maintain the average LC-flow in one direction during the filling process. Then the LC was slowly cooled down in the nematic phase. The micrograph in Fig. 3(a) shows that LC gains a uniformed planar-aligned state, with $\hat{n}$ at 45° with the crossed polarizers, in-between the two WSe_2 monolayers in the WSe_2-based cell. Also, as expected, the LC does not achieve homogeneous alignment where there are two bare ITO layers are present in the cell. After the cell is rotated counterclockwise through 45° under the crossed-polarized microscope, the uniform planar-aligned LC in-between the two WSe_2 monolayers exhibits a dark uniform texture with $\hat{n}$ at 0° with respect to the polarizer, as shown in the micrograph in Fig. 3(b).

To realize the LC's planar-alignment quality in this WSe_2-based cell, the cell was rotated under the crossed-polarized microscope, and the change in the transmitted intensity only through the WSe_2 region of the cell was recorded at every 2° rotation-step. The results are presented in Figs. 3(c), 3(d), 3(e), and 3(f). The angle between the average LC director, $\hat{n}$ and the analyzer is defined by θ. Figures 3(c), 3(d), and 3(e) are the micrographs of the LC texture in the WSe_2-based cell, where $\theta = 0°$, 22.5°, and 45°, respectively. The graph in Fig. 3(f) shows the normalized transmitted intensity of the WSe_2-based LC cell under the crossed-polarized microscope as a function of θ. This transition of the transmitted intensity from a uniform dark texture to a uniform bright texture at every 45° rotation confirms that the two WSe_2 monolayers can impose homogeneous alignment on the LC inside the device. Figure 3(g) shows the picture of the WSe_2-based LC cell.

Optical Materials EXPRESS

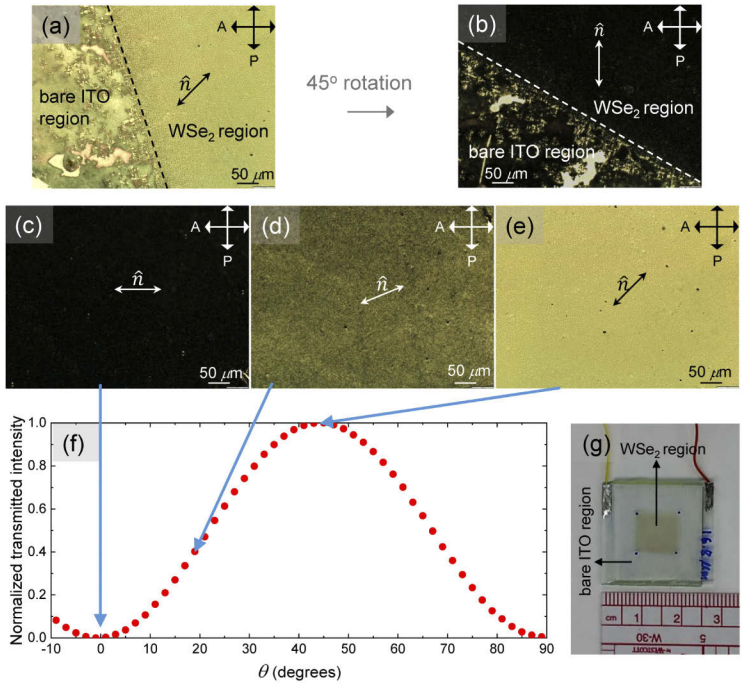

Fig. 3. (a), (b) Crossed-polarized micrograph and its 45° rotated state, respectively, of the WSe_2-based LC cell showing uniform planar-alignment of the LC in the WSe_2 region and unaligned LC in the bare ITO region. (c), (d), and (e) Micrographs of the dark, intermediate, and bright states, respectively, as the WSe_2-based LC cell was rotated under the crossed-polarized optical microscope. (f) Normalized transmitted intensity through the WSe_2-based LC cell as a function of angle θ. (g) The picture of the WSe_2-based LC cell.

2.2. *Electro-optical effect of LC in WSe_2-based cell*

The electro-optical effect of LC E7 in the WSe_2-based cell was studied using an optical setup where the cell was mounted between two crossed polarizers, and $\hat{n}$ in the cell was oriented at 45° with respect to the crossed polarizers. A 5-mW He-Ne laser beam of wavelength 633 nm was sent through the polarizer, the WSe_2-based LC cell, the crossed analyzer, and into a photodetector, which was fed into a dc voltmeter to measure the transmitted intensity. The applied ac voltage at $f = 1000$ Hz across the cell was gradually ramped up, and the change in the transmitted intensity was detected from the dc voltmeter. The same experiment was also carried out under the crossed polarized microscope with a white light source, and several micrographs of the WSe_2-based LC cell at different applied voltages were taken. When the applied voltage across the cell exceeds Fréedericksz threshold value, $\hat{n}$ rotates from the initial planar orientation to homeotropic orientation, and the LC's effective birefringence, $<\Delta n>$ changes as a function of the applied voltage. In our optical setup, $\hat{n}$ is initially oriented at 45° with the crossed polarizers. Therefore, if I_o is the intensity of the plane-polarized light incident on the WSe_2-based LC cell, then the transmitted optical intensity, I at the exit of the analyzer shows an oscillatory behavior according to the equation [25]

$$I = I_O \sin^2\left(\frac{\pi d \langle \Delta n \rangle}{\lambda}\right) \tag{1}$$

where λ is the wavelength of the laser beam and d is the cell-gap.

Optical Materials EXPRESS

Figure 4 represents the electro-optical effect of LC E7 in the WSe_2-based LC cell. Figure 4(a) exhibits the oscillatory response of the transmittance, I/I_o of LC E7 in the WSe_2-based LC cell as a function of the applied ac voltage according to Eq. (1).

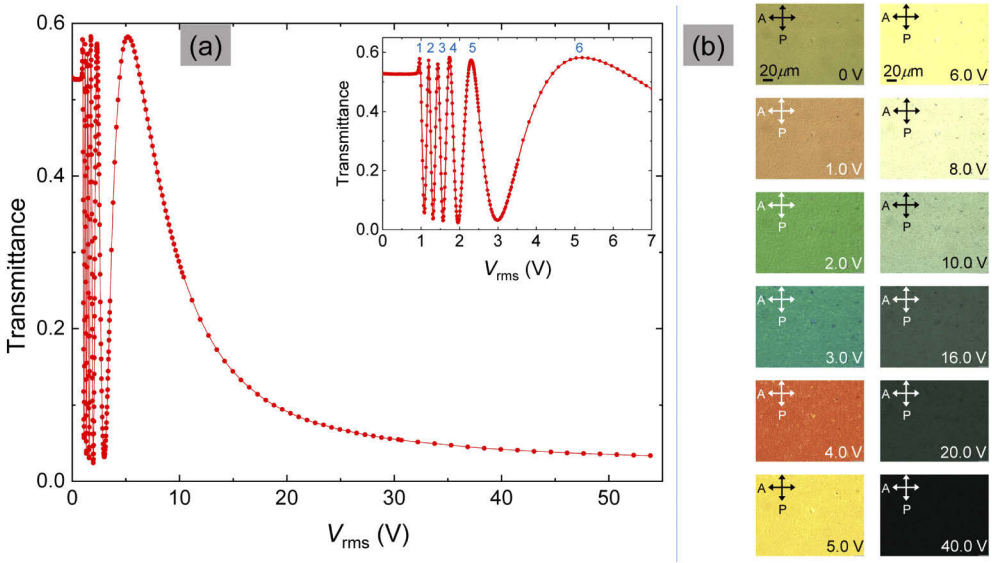

Fig. 4. (a) The transmittance, I/I_o of LC E7 ($T = 22°$ C) in the WSe_2-based LC device as a function of applied ac voltage ($f = 1000$ Hz). A smaller voltage range of the same transmittance curve is shown in the inset, where six maxima can be clearly counted. (b) Twelve separate micrographs of the WSe_2-based LC cell under the crossed-polarized optical microscope at different applied voltages.

The number of maxima appearing in the transmittance curve in Fig. 4(a) is given by ($d\,\Delta n/\lambda$) [25]. Using $\Delta n = 0.225$ for LC E7, $\lambda = 633$ nm for the He-Ne laser and, the WSe_2-based LC cell-gap, $d = 16.8$ μm, we obtain ($d\,\Delta n/\lambda$) ≈ 6. The transmittance curve in a smaller voltage range in the inset in Fig. 4(a) shows six maxima—which confirms a complete director rotation from the planar state to the homeotropic state in the WSe_2-based LC cell. The inset also shows a sharp Fréedericksz transition ($V_{th} = 0.88$ V), indicating that the 2D WSe_2 is able to supply the required amount of planar-anchoring strength as the alignment agent in the cell. Figure 4(b) shows the micrographs of the LC texture in the WSe_2-based LC cell under the crossed-polarized microscope at different applied voltages. The results indicate that the WSe_2-based LC cell exhibits the essential electro-optical effect for a transmissive LC device—where the 2D WSe_2 is employed as the planner-alignment agent.

2.3. Optical transmission spectroscopy of the WSe_2/ITO slide

The optical transmission spectra of a standard PI/ITO substrate and the WSe_2/ITO substrate were studied using FLAME-S-XR1-ES (*Ocean Optics*, *Inc.*) spectrometer in the wavelength range from 300 nm to 1000 nm. A standard planar PI material, KPI-300B (60 nm thick layer on an ITO slide) was used for the PI/ITO slide. The transmission spectra for these two slides are shown in Fig. 5. The thickness of monolayer WSe_2 is ~ 0.6 nm. Replacing the PI layer by monolayer WSe_2 reduces the alignment layer thickness from 60 nm to well below 1 nm. Recent studies using density functional theory calculations suggest that various monolayer 2D materials, including WSe_2, show low absorbance, low reflectance, and high transmittance in the visible spectrum [26]. Therefore, as expected, the WSe_2/ITO substrate shows more optical transparency

Optical Materials EXPRESS

than the standard PI/ITO substrate. Thus, replacing the PI alignment agent by 2D WSe_2 should minimize the transmissive losses over a wide spectral range in the LC device.

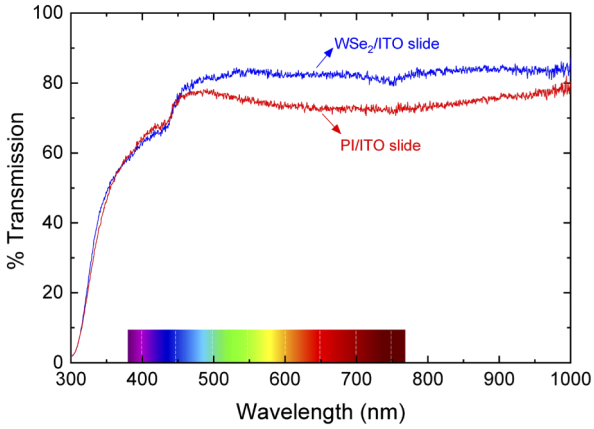

Fig. 5. Optical transmission spectroscopy for WSe_2/ITO slide and PI/ITO slide. The color band on the *x*-axis shows the visible wavelength range.

3. Conclusion

The appearance of the homogeneous alignment of the LC on the WSe_2 film and its absence on bare ITO substrate is a clear indication that 2D WSe_2 can serve as the planar-alignment agent in an LC cell. This WSe_2-based LC cell shows a sharp Fréedericksz transition with the standard electro-optical effect when an electric field is applied across the cell. The higher optical transparency of 2D WSe_2 has potential applications in modern transmissive electro-optic LC devices. Future studies will involve measurements of polar anchoring energy, azimuthal anchoring energy, voltage holding ratio, and residual dc charge of the WSe_2-based LC cell.

Funding

Office of Naval Research (N0001420WX01630, N0001420WX01656, N0001420WX01703); U.S. Naval Academy (Kinnear Fellowship Award).

Disclosures

The authors declare that there are no conflicts of interest related to this article.

References

1. H. C. P. Movva, A. Rai, S. Kang, K. Kim, B. Fallahazad, T. Taniguchi, K. Watanabe, E. Tutuc, and S. K. Banerjee, "High-mobility holes in dual-gated WSe_2 field-effect transistors," ACS Nano **9**(10), 10402–10410 (2015).
2. B. Fallahazad, H. C. P. Movva, K. Kim, S. Larentis, T. Taniguchi, K. Watanabe, S. K. Banerjee, and E. Tutuc, "Shubnikov-de Haas oscillations of high-mobility holes in monolayer and bilayer WSe_2: Landau level degeneracy, effective mass, and negative compressibility," Phys. Rev. Lett. **116**(8), 086601 (2016).
3. R. Bertoni, C. W. Nicholson, L. Waldecker, H. Hübener, C. Monney, U. De Giovannini, M. Puppin, M. Hoesch, E. Springate, R. T. Chapman, C. Cacho, M. Wolf, A. Rubio, and R. Ernstorfer, "Generation and evolution of spin-, valley-, and layer-polarized excited carriers in inversion-symmetric WSe_2," Phys. Rev. Lett. **117**(27), 277201 (2016).
4. Z. Yao, J. Liu, K. Xu, E. K. C. Chow, and W. Zhu, "Material synthesis and device aspects of monolayer tungsten diselenide," Sci. Rep. **8**(1), 5221 (2018).
5. K. Takatoh, M. Hasegawa, M. Koden, N. Itoh, R. Hasegawa, and M. Sakamoto, *Alignment Technology and Applications of Liquid Crystal Devices* (Taylor & Francis, 2005).
6. H.-S. Park and K.-C. Shin, "Liquid crystal cell process," in *Flat Panel Display Manufacturing*, Jun Souk, Shinji Morozumi, Fang-Chen Luo, and Ion Bita, eds. (John Wiley & Sons, Ltd., 2018).

Optical Materials EXPRESS

7. N. A. J. M. Van Aerle, "Influence of polyimide orientation layer material on the liquid crystal resistivity in LCDs," Mol. Cryst. Liq. Cryst. Sci. Technol., Sect. A **257**(1), 193–208 (1994).
8. C.-H. Wen, S. Gauza, and S.-T. Wu, "Photostability of liquid crystals and alignment layers," J. Soc. Inf. Disp. **13**(9), 805–811 (2005).
9. Y. J. Lim, Y. E. Choi, S.-W. Kang, D. Y. Kim, S. H. Lee, and Y.-B. Hahn, "Vertical alignment of liquid crystals with zinc oxide nanorods," Nanotechnology **24**(34), 345702 (2013).
10. V. G. Chigrinov, V. M. Kozenkov, and H.-S. Kwok, *Photoalignment of Liquid Crystalline Materials: Physics and Applications* (John Wiley & Sons, Ltd., 2008).
11. T-Z Shen, S-H Hong, J-H Lee, S-G Kang, B. Lee, D. Whang, and J-K Song, "Selectivity of threefold symmetry in epitaxial alignment of liquid crystal molecules on macroscale single-crystal graphene," Adv. Mater. **30**(40), 1802441 (2018).
12. R. Basu and S. Shalov, "Graphene as transmissive electrodes and aligning layers for liquid-crystal-based electro-optic devices," Phys. Rev. E **96**(1), 012702 (2017).
13. R. Basu and A. Lee, "Ion trapping by the graphene electrode in a graphene-ITO hybrid liquid crystal cell," Appl. Phys. Lett. **111**(16), 161905 (2017).
14. R. Basu and L. J. Atwood, "Characterizations of a graphene-polyimide hybrid electro-optical liquid crystal device," OSA Continuum **2**(1), 83–91 (2019).
15. R. Basu and L. J. Atwood, "Two-dimensional hexagonal boron nitride nanosheet as the planar-alignment agent in a liquid crystal-based electro-optic device," Opt. Express **27**(1), 282–292 (2019).
16. R. Basu and L. J. Atwood, "Reduced ionic effect and accelerated electro-optic response in a 2D hexagonal boron nitride planar-alignment agent based liquid crystal device," Opt. Mater. Express **9**(3), 1441–1449 (2019).
17. R. Basu, "Enhancement of effective polar anchoring strength and accelerated electro-optic switching in a two-dimensional hexagonal boron nitride/polyimide hybrid liquid crystal device," Appl. Opt. **58**(24), 6678–6683 (2019).
18. M. A. Shehzad, J. Lee, S. H. Park, I. Akhtar, M. F. Khan, S. Hussain, J. Eom, J. Jung, G. Kim, C. Hwang, and Y. Seo, "Dynamics of liquid crystal on hexagonal lattice," 2D Mater. **5**(4), 045021 (2018).
19. M. A. Shehzad, S. Hussain, J. Lee, J. Jung, N. Lee, G. Kim, and Y. Seo, "Study of grains and boundaries of molybdenum diselenide and tungsten diselenide using liquid crystal," Nano Lett. **17**(3), 1474–1481 (2017).
20. D. W. Kim, J. M. Ok, W.-B. Jung, J.-S. Kim, S. J. Kim, H. O. Choi, Y. H. Kim, and H.-T. Jung, "Direct observation of molybdenum disulfide, MoS_2, domains by using a liquid crystalline texture method," Nano Lett. **15**(1), 229–234 (2015).
21. X. Li, Y. Zhu, W. Cai, M. Borysiak, B. Han, D. Chen, R. D. Piner, L. Colombo, and R. S. Ruoff, "Transfer of large-area graphene films for high-performance transparent conductive electrodes," Nano Lett. **9**(12), 4359–4363 (2009).
22. X. Liang, B. A. Sperling, I. Calizo, G. Cheng, C. A. Hacker, Q. Zhang, Y. Obeng, K. Yan, H. Peng, Q. Li, X. Zhu, H. Yuan, A. R. H. Walker, Z. Liu, L.-M. Peng, and C. A. Richter, "Toward clean and crackless transfer of graphene," ACS Nano **5**(11), 9144–9153 (2011).
23. M. Yang, X. Cheng, Y. Li, Y. Ren, M. Liu, and Z. Qi, "Anharmonicity of monolayer MoS_2, $MoSe_2$, and WSe_2: A Raman study under high pressure and elevated temperature," Appl. Phys. Lett. **110**(9), 093108 (2017).
24. P. Tonndorf, R. Schmidt, P. Böttger, X. Zhang, J. Börner, A. Liebig, M. Albrecht, C. Kloc, O. Gordan, D. R. T. Zahn, S. Michaelis de Vasconcellos, and R. Bratschitsch, "Photoluminescence emission and Raman response of monolayer MoS_2, $MoSe_2$, and WSe_2," Opt. Express **21**(4), 4908–4916 (2013).
25. L. M. Blinov and V. G. Chigrinov, *Electro-optic Effects in Liquid Crystal Materials* (Springer-Verlag, 1996).
26. S. Gupta, S. N. Shirodkar, A. Kutana, and B. I. Yakobson, "In Pursuit of 2D materials for maximum optical response," ACS Nano **12**(11), 10880–10889 (2018).